





# Impact of Polyvinylidene Fluoride on Nanofiber Cathode Structure and Durability in Proton Exchange Membrane Fuel Cells

John J. Slack,<sup>1,a</sup> M. Brodt,<sup>1,b</sup> David A. Cullen,<sup>2,\*</sup> Kimberly S. Reeves,<sup>2</sup> Karren L. More,<sup>2,\*</sup>  and Peter N. Pintauro<sup>1,\*\*,z</sup> 

<sup>1</sup>Department of Chemical and Biomolecular Engineering, Vanderbilt University, Nashville, Tennessee 37212, United States of America

<sup>2</sup>Center for Nanophase Materials Sciences, Oak Ridge National Laboratory, Oak Ridge, Tennessee 37831, United States of America

The impact of polyvinylidene fluoride (PVDF) as a binder component on the durability of Pt/C cathodes in a proton exchange membrane fuel cell membrane-electrode-assembly (MEA) during a carbon corrosion accelerated stress test (AST) was examined using electrochemical fuel cell data and visual inspection/analysis of the cathode morphology via electron-microscopy. Electrospun nanofiber cathode mat MEAs with a Nafion®/PVDF or Nafion/poly(acrylic acid) (PAA) binder or a slurry cathode MEA with neat Nafion or a Nafion/PVDF binder were investigated. The presence of PVDF had profound effects on the structure and chemical/electrochemical properties of a fuel cell cathode; its hydrophobic property slowed the rate of carbon loss and its robust mechanical properties added strength to the binder. Thus, the extent of carbon loss during an AST was inversely proportional to the PVDF content of the binder and there was no observable cathode thinning nor any change in cathode porosity after the AST, when the cathode binder contained at least 50 wt% PVDF. In terms of long-term durability, these beneficial structural effects outweighed the lower Nafion/PVDF binder conductivity and the associated lower initial power output of a Nafion/PVDF cathode MEA. For hydrophilic slurry and nanofiber cathodes with neat Nafion or Nafion/PAA fibers, low power after the carbon corrosion AST was due to greater carbon losses, cathode thinning and the collapse of cathode pores, which dominated MEA performance even though the initial cathode ECSA and mass activity were high for these two MEAs.

© 2020 The Author(s). Published on behalf of The Electrochemical Society by IOP Publishing Limited. This is an open access article distributed under the terms of the Creative Commons Attribution 4.0 License (CC BY, <http://creativecommons.org/licenses/by/4.0/>), which permits unrestricted reuse of the work in any medium, provided the original work is properly cited. [DOI: 10.1149/1945-7111/ab77fb]



Manuscript submitted October 23, 2019; revised manuscript received January 24, 2020. Published March 16, 2020. *This paper is part of the JES Focus Issue on Heterogeneous Functional Materials for Energy Conversion and Storage.*

The durability of the membrane-electrode-assembly (MEA) in a proton exchange membrane fuel cell (PEMFC) has been the subject of numerous studies, involving both the identification of new materials/component as well as new ways to assess long-term performance from a short-term test. Electrode durability in a H<sub>2</sub>/air fuel cell has mainly focused on assessing the effects of precious metal dissolution and carbon corrosion at the cathode. Methods of characterizing durability include electrochemical analyses (long-term fuel cell operation at constant current or voltage<sup>1,2</sup> or a voltage cycling accelerated stress test<sup>3</sup>), morphological observations,<sup>3–5</sup> elemental analyses,<sup>6</sup> and atomic structure analyses.<sup>7</sup> Cathode degradation over time in a MEA is influenced by the type of precious metal catalyst (carbon support material and amount/type/distribution of precious metal), the ionomer binder, and the structure of the ionomer/catalyst interface.<sup>8</sup> The durability of fuel cell cathodes has improved considerably in recent years by modifying<sup>9</sup> or completely eliminating<sup>10</sup> the catalyst carbon support and/or by utilizing a nanofiber mat electrode morphology, which improved the power output after a carbon corrosion start/stop voltage cycling accelerated stress test<sup>11</sup> (AST) and decreased metal dissolution/agglomeration after a load cycling AST.<sup>12</sup> Brodt et al.<sup>13</sup> found that the addition of hydrophobic polyvinylidene fluoride to the Nafion binder of a fiber mat cathode with Pt/C catalyst dramatically improved MEA durability during a carbon corrosion AST by limiting water contact with the catalyst surface, while promoting a high mass activity for oxygen reduction at the end of the test and the facile expulsion of product water from the cathode during the AST. The Nafion/PVDF binder work was a continuation of initial studies on electrospun nanofiber electrodes for PEMFCs<sup>14–16</sup> where a hydrophilic Nafion/poly(acrylic acid) cathode binder was employed and where the cathodic electrochemical surface area and oxygen reduction

reaction mass activity were high. The present study was undertaken to further examine and explain the improved carbon corrosion durability of H<sub>2</sub>/air fuel cell nanofiber mat and slurry cathodes containing a Nafion/PVDF binder, with a focus on the physical structure of the cathode before and after voltage cycling.

The structure of the catalyst layer in a conventional slurry cathode after a carbon corrosion voltage cycling AST has been the subject of numerous research papers, which focused on catalyst particle coarsening/agglomeration, the generation of carbon-oxygen moieties on the carbon support which made the cathode more hydrophilic and prone to flooding, a decrease in the electrical conductivity of the catalyst support, a decrease in graphitic content of the support, a change in the cathode pore size distribution, and a decrease in overall catalyst layer thickness.<sup>17–20</sup> The work of Uchida et al.<sup>21</sup> is of particular importance wherein the authors describe PEMFC catalyst layers as having two distinctive pore size distributions: primary pores with a diameter smaller than 0.1 μm and secondary pores with a diameter larger than 0.1 μm. During a carbon corrosion voltage cycling AST, secondary pores were found to collapse in size with a decrease in the overall cathode catalyst layer thickness. The phenomena of pore collapse and cathode thinning have been specifically addressed in the present study, using a series of nanofiber and slurry cathode MEAs containing either neat Nafion, Nafion/poly(acrylic acid) (PAA), or Nafion/PVDF as the cathode catalyst binder. Nanostructure imaging analyses were employed to assess the cathode structure before and after a carbon corrosion AST, using testing protocols defined by the U.S. Department of Energy.<sup>22</sup> Images were related to fuel cell polarization data, electrochemically active surface area (ECSA), and cathode catalyst mass activity for oxygen reduction. We show that the use of PVDF in a mixed polymer binder with Nafion helps to preserve the cathode structure and better retain beginning-of-life power after a carbon corrosion voltage cycling accelerated stress test.

## Experimental

**MEA preparation and AST experiments.**—Nanofiber and slurry cathode MEAs were identical to those prepared and used by

\*Electrochemical Society Member.

\*\*Electrochemical Society Fellow.

<sup>a</sup>Present address: Nikola Motor Company, Phoenix, Arizona 85040, United States of America.

<sup>b</sup>Present address: Helmholtz Institute for Renewable Energy, Erlangen, Germany.

<sup>z</sup>E-mail: [pn.pintauro@vanderbilt.edu](mailto:pn.pintauro@vanderbilt.edu)

**Table I. Cathode compositions and cathode ink solvents for nanofiber and slurry MEAs, where the cathode Pt loading is 0.10 mg/cm<sup>2</sup>.**

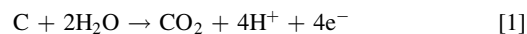
Dry Cathode Composition (weight %)	Cathode Type	Ink solvents
70 catalyst/30 PVDF	nanofiber	DMF/acetone
70 catalyst/10 Nafion/20 PVDF	nanofiber	DMF/THF/acetone
70 catalyst/15 Nafion/15 PVDF	nanofiber	DMF/THF/acetone
70 catalyst/24 Nafion/6 PVDF	nanofiber	DMF/THF/acetone
64 catalyst/24 Nafion/12 PAA	nanofiber	Isopropyl alcohol/water
70 catalyst/15 Nafion/15 PVDF	slurry	DMF/THF/acetone
64 catalyst/24 Nafion/12 PAA	slurry	Isopropyl alcohol/water
70 catalyst/30 Nafion	slurry	Isopropyl alcohol/water

Brodth et al. in Ref. 13. Johnson Matthey Pt supported on HiSpec 4000 carbon was used as the cathode catalyst. Inks for electrospinning were prepared with Kynar HSV 900 polyvinylidene fluoride (Arkema, Inc.) and dried 1100 EW Nafion resin (Nafion powder was obtained by evaporating a liquid dispersion from Ion Power, Inc.). The solids content (catalyst and binder) of an electrospinning ink was 15 wt%, whereas slurry inks contained 5 wt% solids. The final cathode compositions and the solvent components used to prepare the eight cathode inks used in the present study are listed in Table I. For inks containing PVDF as one of the cathode binder components, the solvent system was either a dimethylformamide (DMF)/acetone mixture or a DMF/tetrahydrofuran (THF)/acetone mixture. Nanofiber and slurry cathode inks with Nafion + poly(acrylic acid) (PAA) and a slurry cathode ink with neat Nafion utilized a solvent of isopropyl alcohol and water. Inks were prepared as follows: catalyst and high-boiling solvent (either DMF or water) were combined and the mixture was sonicated for 30 min. Next, additional solvent and all polymer components were added and the mixture was sonicated for an additional hour. Finally, the ink was mixed overnight using a mechanical stirrer. Inks for electrospinning were drawn into a 3 ml syringe, capped with a 22 gauge metal needle, and placed into a syringe pump as part of an electrospinning apparatus that has been described previously.<sup>13,14,23</sup> For PVDF-containing inks, well-formed electrospun fibers were created in high relative humidity air (50%–70% RH) at ambient temperature, with a rotating and horizontally oscillating drum collector, a needle-to-collector distance of 10 cm, a syringe pump flow rate of 1.0 ml/hr, and a voltage bias in the range of 12–15 kV. All cathodes with PVDF contained 70 wt% catalyst, with a fixed ionomer-to-carbon ratio of 0.88 (where the ionomer content is the sum of Nafion and PVDF polymers). For Nafion + PAA fibers, the (Pt/C)/Nafion/PAA wt% composition was 64/24/12 and the ionomer to carbon ratio was 1.2 (here ionomer was defined as Nafion + PAA). Fiber electrospinning was carried out using a rotating drum collector with a needle-to-collector distance of 8 cm, an ink flow rate of 0.8 ml/hr, an applied voltage of 10.5 kV, and a relative humidity and air temperature of 40% RH and 22 °C. For all nanofiber cathode MEAs, the anode was an electrospun 64/24/12 (Pt/C)/Nafion/PAA fiber mat. Catalyst coated membranes with nanofiber electrodes were fabricated by hot pressing 5 cm<sup>2</sup> electrospun nanofiber mats onto the surfaces of a Nafion 211 membrane at 140 °C and 4 MPa for 2 min. Carbon paper gas diffusion layers (GDLs) (Sigracet 25 BC GDL) were physically pressed onto the anode and cathode of a CCM while in the fuel cell test fixture to form an MEA. The cathode and anode catalyst loading was held constant at 0.1 mg<sub>Pt</sub>/cm<sup>2</sup>.

Slurry cathodes were prepared by painting an ink with either neat Nafion or Nafion/PVDF onto Sigracet 25 BC carbon paper followed by hot-pressing onto a Nafion 211 membrane. The ink composition for Nafion/PVDF binders was identical to that used for electrospinning. All painted GDEs (5 cm<sup>2</sup> in geometric area) were hot pressed onto a Nafion 211 membrane (along with a nanofiber anode) at 140 °C and 4 MPa for 2 min after a 10 min pre-heating step at 140 °C with no applied pressure (same conditions as those used for nanofiber cathode/anode MEAs).

**Electrochemical testing of MEAs.**—MEAs were evaluated on a Scribner Associates Inc. 850e single cell test station using a fuel cell test fixture with single serpentine H<sub>2</sub> and air flow channels. MEAs were conditioned at 80 °C and ambient pressure by alternating potentiostatic and galvanostatic holds for two minutes each at 150 mA/cm<sup>2</sup> and 0.2 V until steady-state operation was achieved (ca. 3 h) with fully humidified H<sub>2</sub> gas and air fed to the anode and cathode at 125 sccm and 500 sccm, respectively. Beginning-of-life (BOL) operation of the MEA was defined immediately after break in. H<sub>2</sub>/air fuel cell polarization data were collected at ambient pressure and 80 °C, with fully humidified hydrogen and air streams at flow rates of 125 sccm and 500 sccm, respectively. Cathode mass activity was measured at 150 kPa<sub>abs</sub>, 80 °C, and 100 sccm each for H<sub>2</sub> and O<sub>2</sub> using a current-controlled scan from high to low current (1.0 to 0.01 Amps at four points/decade). Mass activities were determined as current normalized to mass (for a loading of 0.1 mg<sub>Pt</sub>/cm<sup>2</sup>) at 0.9 V by plotting the IR-free voltage, corrected for high frequency resistance (measured in a separate experiment), against the hydrogen-crossover-corrected current density.<sup>24</sup> Electrochemical surface area was obtained from the area under a cyclic voltammogram corresponding to hydrogen adsorption, when the fuel cell was operating at 30 °C and 100% RH with a nitrogen-purged cathode and a hydrogen gas feed of 100 sccm at the anode.<sup>25</sup>

After collecting BOL data, MEAs underwent a carbon corrosion accelerated stress test (AST). As originally outlined by the fuel cell commercialization conference of Japan<sup>26</sup> and the U.S. Department of Energy,<sup>22</sup> the voltage at the cathode was cycled between 1.0 and 1.5 V at a scan rate of 500 mV/s using a triangular voltage wave for 1,000 cycles (a sufficient number of cycles to distinguish the effect of cathode composition and morphology on durability). The fuel cell operating conditions during the AST were 80 °C, ambient pressure, and fully humidified (100% RH) feed-gases (125 sccm hydrogen at the anode and 250 sccm nitrogen at the cathode). An external potentiostat (Gamry Instruments Reference 3000) was used to cycle the voltage. For the duration of the AST, as the cathode carbon support was oxidized according to Eq. 1, the CO<sub>2</sub> in the cathode air exhaust was monitored, using an infrared carbon dioxide detector from CO<sub>2</sub> Meter Inc. (Model No. CM-0152).



**Electron microscopy characterization.**—The MEAs listed in Table I were characterized by Scanning Electron Microscopy (SEM) and Scanning Transmission Electron Microscopy (STEM) at beginning-of-life (BOL) and end-of-life (EOL, also referred to in the literature as end-of-test) in terms of cathode catalyst layer (CL) thinning and changes in cathode porosity and pore-size distribution. Samples were prepared for analysis by diamond-knife ultramicrotomy. For each sample, a MEA cross-section approximately 100 microns in thickness was imaged using a Hitachi S4800 scanning electron microscope with an yttrium aluminum garnet (YAG) scintillator detector for backscatter electrons (BSE). Across a

section of MEA, three 10,000 $\times$  magnification images were taken of the CL to obtain a representative average thickness and to measure variations in thickness along the CL, i.e., in the direction parallel to the electrode/membrane interface. Each image was analyzed for electrode thickness using FIJI ImageJ software at 15 locations along the electrode (a total of 45 separate measurements for the three images) to obtain a statistically significant value of thickness for each cathode. The same procedure was performed on MEAs at BOL and EOL. Scanning transmission electron microscopy data were collected using a FEI Talos F200X instrument to obtain high-resolution images of the cathode cross-section at BOL and EOL for electrode porosity determinations. The porosity and pore-size distribution in a cathode were extracted from STEM images using FIJI ImageJ software. Images were first binarized such that each pixel returned either a signal of black or white, where white pixels corresponded to solid particles (either platinum, carbon, Nafion, or PVDF) and black pixels corresponded to void-space. The void space areas were summed up using a “classic watershed” algorithm which is designed to mark boundaries of regions that are segmented based on pixel intensity.<sup>27</sup>

## Results and Discussion

**Catalyst layer thinning.**—A decrease in the thickness of the cathode catalyst layer (CL) after carbon corrosion voltage cycling indicates several types of damage, including the loss of carbon via oxidation to CO<sub>2</sub>, and collapse of pores.<sup>28</sup> These changes affect the electrochemical performance of the cell by reducing ECSA (increasing activation overpotential) and inhibiting access of oxygen to catalyst sites (increasing cathode hydrophilicity, resulting in flooding and an increase in mass transport resistance/overpotential).<sup>29</sup> Measuring the CL thickness of each cathode in Table I provides a

deeper understanding of how PVDF in the cathode binder affects electrode durability. Figures 1a and 1b show BSE SEM cross-sections of a conventional slurry electrode with neat Nafion at BOL and EOL. The cathode thickness decreased by more than 50% at EOL which is consistent with previously published data,<sup>28,30,31</sup> e.g., Watanabe and coworkers who observed a catalyst layer thickness reduction of 53% with Pt detachment from the carbon support and Dubau et al. who observed a reduction in electrical conductivity of the cathode due to an increase in carbon-oxygen moieties, and membrane failure near the thinnest portions of the cathode.

Figures 1c and 1d show BSE SEMs of a slurry cathode with a binder of 1/1 Nafion/PVDF at beginning-of-life and at end-of-test. In these images, there is no statistically significant change in the CL thickness. Given that the same type of carbon was used in the electrodes of Figs. 1a, 1b and 1c, 1d, the retention of the original catalyst layer thickness was associated with the addition of PVDF to the Nafion binder. Figures 1e and 1f show BSE SEMs of a nanofiber cathode MEA with no PVDF at BOL and EOL (a standard Nafion/PAA binder as per Brodt et al.<sup>13,15,16</sup>), which also underwent significant (>50%) thinning after the AST. In Figs. 1g and 1h, BSE SEMs of a nanofiber electrode with a binder of 1/1 Nafion/PVDF, show no change in the CL thickness after carbon corrosion voltage cycling. It can be concluded, based on these images, that a 1/1 Nafion/PVDF cathode binder (i.e., a Nafion binder containing 50 wt% PVDF) stabilizes the structure/morphology of a Pt/C fuel cell cathode (both a slurry cathode or a nanofiber cathode).

The preservation of cathode thickness is associated with an improvement in power density retention after a carbon corrosion AST for both nanofiber and slurry cathode MEAs, when PVDF is added to Nafion in the cathode, as shown by Brodt et al.<sup>13</sup> As an example of this correlation, H<sub>2</sub>/air fuel cell polarization curves are compared in Fig. 2 for nanofiber electrode MEAs with either a

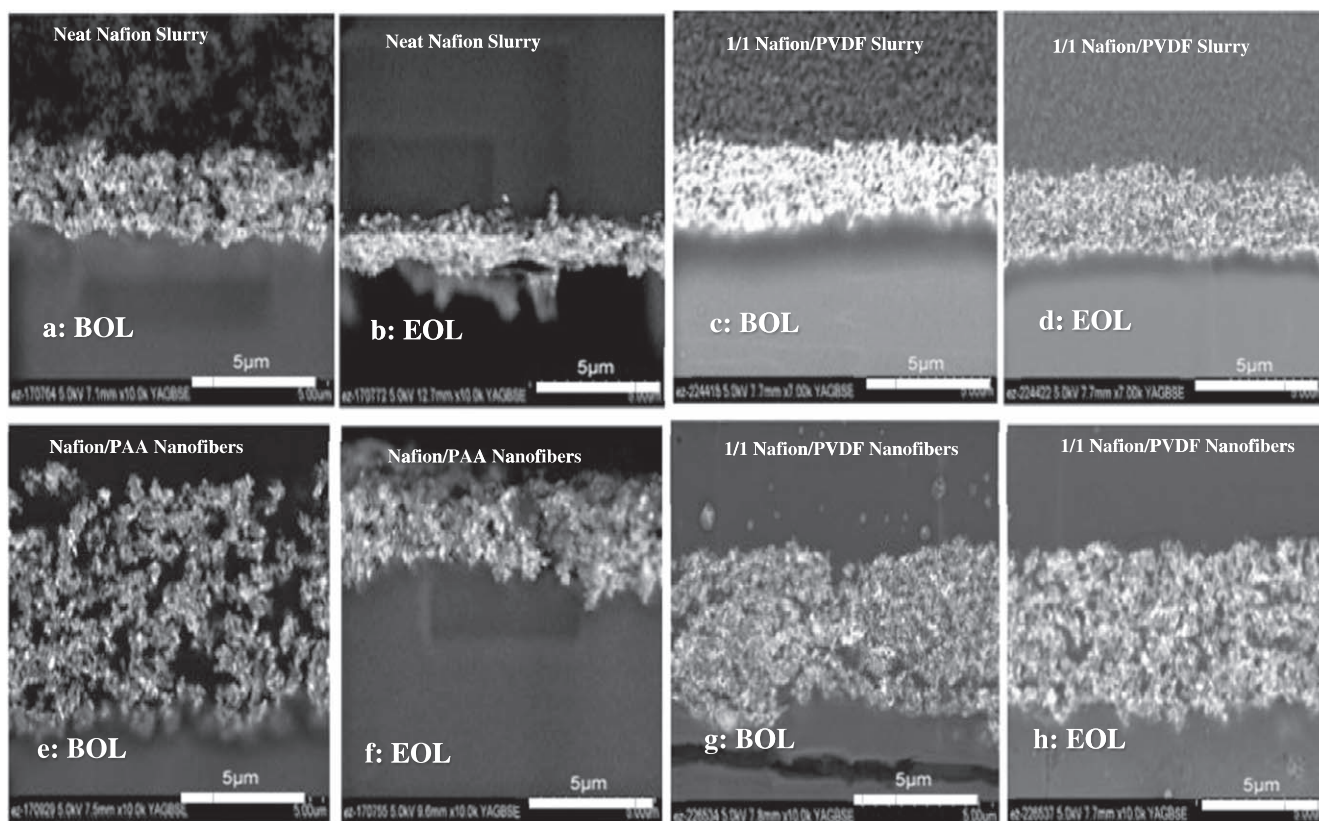


**Figure 1.** Representative cross-sectional back-scatter SEM images of cathode catalyst layers in an MEA: (a) BOL neat Nafion slurry, (b) EOL neat Nafion slurry, (c) BOL 1/1 Nafion/PVDF slurry, (d) EOL 1/1 Nafion/PVDF slurry (e) BOL Nafion/PAA Nanofibers (0% PVDF) (f) EOL Nafion/PAA nanofibers (0% PVDF) (g) BOL 1/1 Nafion/PVDF nanofibers, and (h) EOL 1/1 Nafion/PVDF nanofibers.



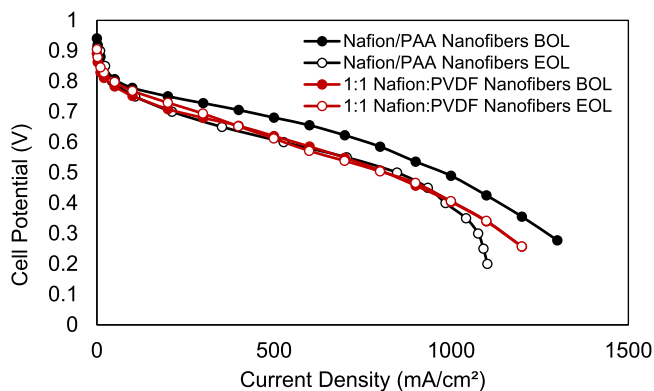


**Figure 2.** Polarization data for nanofiber cathode MEAs with 2:1 Nafion/PAA binder or 1/1 Nafion/PVDF binder. EOL is after 1,000 carbon corrosion voltage cycles from 1.0 V–1.5 V at 500 mV/s in a triangular wave. All MEAs have cathode and anode loadings of 0.1 mg<sub>Pt</sub>/cm<sup>2</sup>. A Nafion 211 membrane and Sigracet 25BC gas diffusion layers were used in all MEAs. The fuel cell operating conditions are 80 °C, ambient pressure, and 125/500 sccm H<sub>2</sub>/air feed gas flow rates.

Nafion/PAA or 1/1 Nafion/PVDF binder. For the Nafion/PVDF binder, power densities at BOL and EOL are lower than those for Nafion/PAA, due to the presence of PVDF, which makes the cathode catalyst surface drier and dilutes the Nafion binder with uncharged polymer, thus lowering the binder conductivity, but the use of PVDF improves the power output stability. The lower power of non-PVDF-based electrodes after the AST in Fig. 3 was attributed to a decrease in cathode thickness and porosity.

In Fig. 3, a summary is presented of nanofiber cathode thinning and cathode carbon loss (as measured by the integrated total amount of CO<sub>2</sub> in the air exhaust during an AST) as a function of PVDF content in a Nafion/PVDF binder. Significant cathode thinning occurs when the PVDF content in the cathode binder is < 50%, where the carbon loss is > 12 wt%. The fact that there is essentially no loss in cathode thickness for a binder with 50% PVDF, even though there is a measured 12% loss in carbon content suggests that PVDF is effectively maintaining the structural integrity of the CL, thus preventing electrode collapse. It should be noted that the error bars in Fig. 3 were determined by multiplying the standard error (standard deviation/sample size) with the z-value for 95% confidence followed by normalizing to the mean of the thicknesses for each cathode. The statistical significance of the measured CL thicknesses was evaluated using analysis of variance (ANOVA), where the variance of the total measurements was compared to the variance within each MEA CL dataset and to the variance between each MEA CL dataset ( $p < 0.01$ ). The large error bars (uncertainties) in CL thickness at low PVDF contents was due to non-uniform thinning. It should also be noted that Brodt et al.<sup>13</sup> found that the

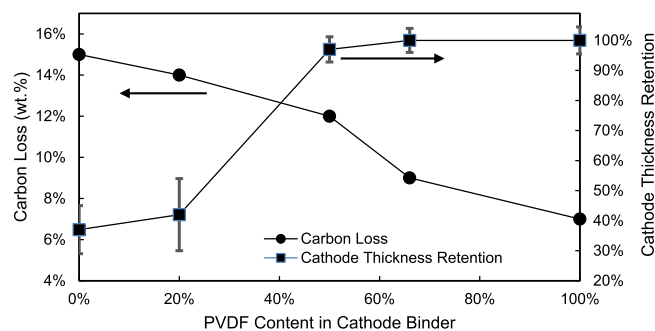


**Figure 3.** Nanofiber electrode carbon loss and retention of cathode thickness as a function of PVDF content. Carbon loss data obtained from Brodt et al.<sup>13</sup>

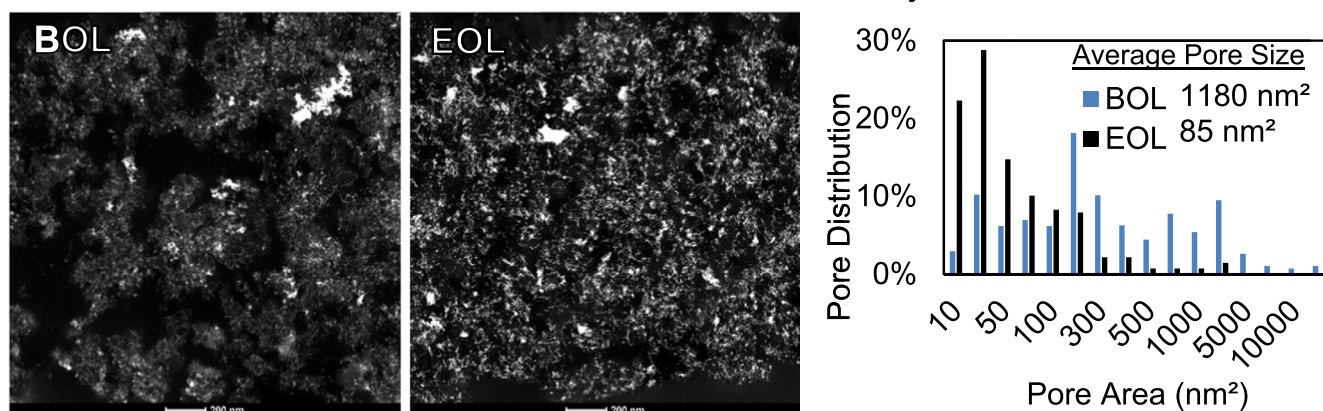
carbon loss in slurry and nanofiber cathodes was the same for a given Nafion/PVDF binder composition, i.e., the wt% carbon loss in Fig. 3 represents the degradation of either a slurry or nanofiber cathode after an AST.

While there is qualitative consistency between CO<sub>2</sub> generation (cathode carbon loss) and catalyst layer thinning for both slurry and nanofiber cathodes, fuel cell power losses were always greater for a slurry cathode relative to a nanofiber electrode for the same Nafion/PVDF composition.<sup>13</sup> This difference is attributed to the highly desirable characteristics of a nanofiber fuel cell electrode, i.e., intra- and inter-fiber porosity and the conformal coating of binder on catalyst particles (with no visible agglomerates of binder or catalyst) which allows for low gas transport resistance, facile water removal, and a high electrochemical surface area (ECSA).

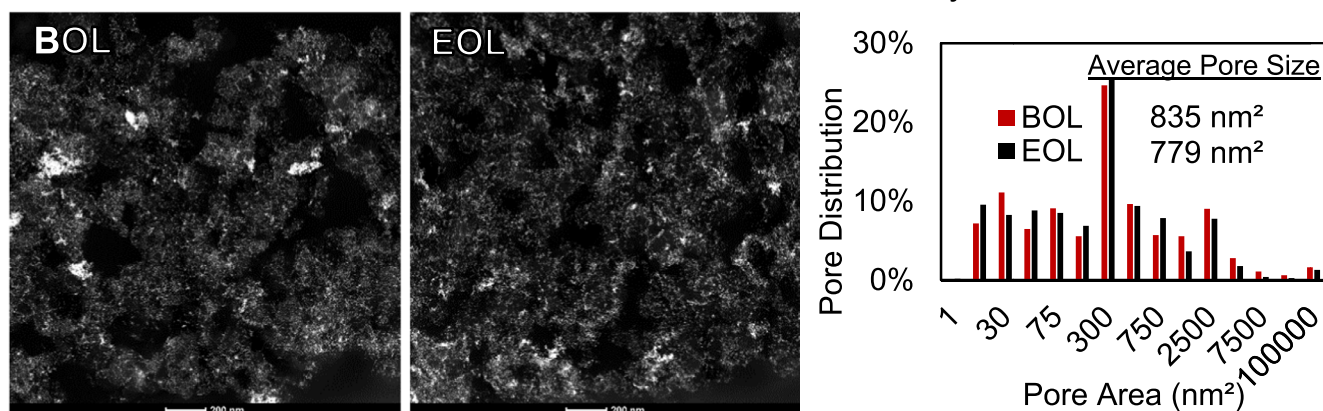
Prior researchers have found that one can mitigate the effects of catalyst layer thinning through the use of different catalyst supports, e.g., Castanheira et al.,<sup>32</sup> who used graphitic carbon, Ramani and coworkers<sup>33</sup> who have been examining oxide supports, or by completely eliminating the support material as is the case with 3M Company's nanostructured thin film electrodes.<sup>34</sup> While graphitized carbon supports better retain surface area during durability tests,<sup>33</sup> they often have a lower ECSA due to a hydrophobic surface that results in a non-optimal Pt distribution.<sup>35</sup> The latter approach is in stark contrast with the use of a Nafion/PVDF binder with a nanofiber electrode morphology which does not reduce the electrochemically active surface area at BOL, as was shown by Brodt et al.<sup>13</sup> Depending on the PVDF content in a Nafion/PVDF binder, a nanofiber cathode loses 20%–35% of its initial ECSA after a carbon corrosion AST, which is similar to the ECSA loss of a fully graphitic carbon support and much lower than a conventional high surface area carbon support which can lose up to 80% of its initial ECSA after a carbon corrosion AST.<sup>32</sup>

**Porosity measurements.**—The pore area distribution of slurry and nanofiber mat cathodes was obtained directly from digitized STEM images of electrode cross-sections at BOL and EOL. Cathode porosity was calculated as the ratio of the total pore and electrode areas. Figure 4 shows BOL and EOL STEM cross-section images with a neat Nafion slurry cathode, a 1/1 Nafion/PVDF slurry cathode, and a nanofiber cathode with a 1/1 Nafion/PVDF binder. Next to each pair of images is a histogram showing the calculated pore area distribution from each cathode at BOL and EOL. Fuel cell polarizations plots at BOL and EOL for the same cathodes are shown in Fig. 5. The mean pore area for the neat Nafion slurry cathode decreased significantly at EOL, from 1180 nm<sup>2</sup> to 85 nm<sup>2</sup>, whereas the mean pore area for the 1/1 Nafion/PVDF slurry cathode remained essentially constant (835 nm<sup>2</sup> at BOL vs 779 nm<sup>2</sup> at EOL). The mean pore area for the 1/1 Nafion/PVDF nanofiber electrode, was initially high and increased slightly from 950 nm<sup>2</sup> to 1025 nm<sup>2</sup> after the carbon corrosion AST (at the present time, we believe that this increase in porosity is real and not associated with data analysis errors). Additional porosity data are listed in Table II, for slurry cathodes with neat Nafion and Nafion/PVDF binder and nanofiber mat cathodes with a Nafion/PVDF binder. A Nafion/PAA nanofiber cathode MEA is also listed as a reference. Table II also has BOL and EOL power densities and the observed changes in cathode thickness. Retention of electrode porosity is desirable and associated with improved MEA mass transport properties, i.e., oxygen transport to catalytic sites and water removal from the cathode, which is known to improve fuel cell power output.<sup>35,36</sup> Additionally, the average pore size at EOL is larger for the nanofiber electrode with Nafion/PVDF as compared to a slurry electrode with the same binder, which explains the difference in performance seen at EOL for these two electrodes (Fig. 5), where larger pores (i.e. secondary pores as described by Watanabe and coworkers<sup>30</sup>) act as channels that allow for improved oxygen access to Pt catalyst sites and better water removal. The combined results in this section show that: (1) both nanofiber and slurry cathodes with Nafion/PVDF binder retain their

## a. Neat Nafion Slurry



## b. 1/1 Nafion/PVDF Slurry



## c. 1/1 Nafion/PVDF Nanofibers

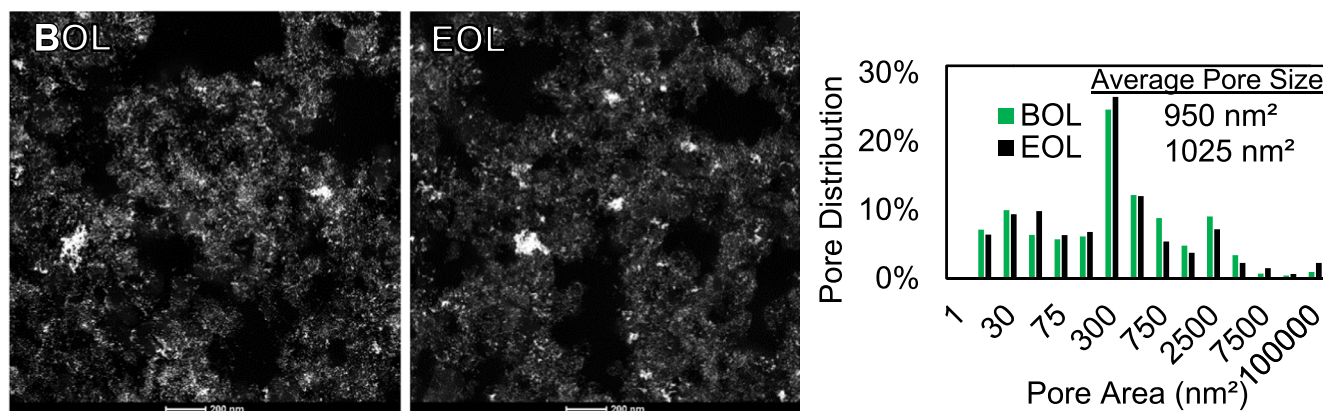


**Figure 4.** STEM imaging analysis of pore area distribution for the BOL and EOL (1000 carbon corrosion voltage cycles) accompanied by a BOL/EOL histogram of pore area distribution for (a) neat Nafion slurry electrode, (b) 1/1 Nafion/PVDF slurry electrode and (c) 1/1 Nafion/PVDF nanofiber electrode.

thickness and porosity after a carbon corrosion AST and (2) a slurry cathode with neat Nafion binder and a nanofiber cathode with Nafion/PAA binder collapse after carbon corrosion with a loss in both porosity and thickness. As can be seen in Fig. 5, the BOL performance of a nanofiber cathode MEA with Nafion/PVDF is about the same as that for a slurry electrode with neat Nafion, so there is no powder density penalty at BOL when using a more hydrophobic Nafion/PVDF binder,<sup>37</sup> i.e., the drop in power due to the low proton conductivity of a Nafion/PVDF binder<sup>13</sup> is offset by

the higher cathode ECSA and oxygen reduction mass activity that characterizes nanofiber cathodes. It also appears that PVDF acts as a reinforcing scaffold for the cathode, preventing its collapse during carbon corrosion, even as the cathode is losing some carbon and becoming more porous.

The differences in MEA performance at BOL and EOL for the fiber and sprayed cathode MEAs in Fig. 5 are best explained by combining the cathode thickness and porosity data in Table II with ECSA and mass activity data in Table III (data from Ref. 13). Thus,

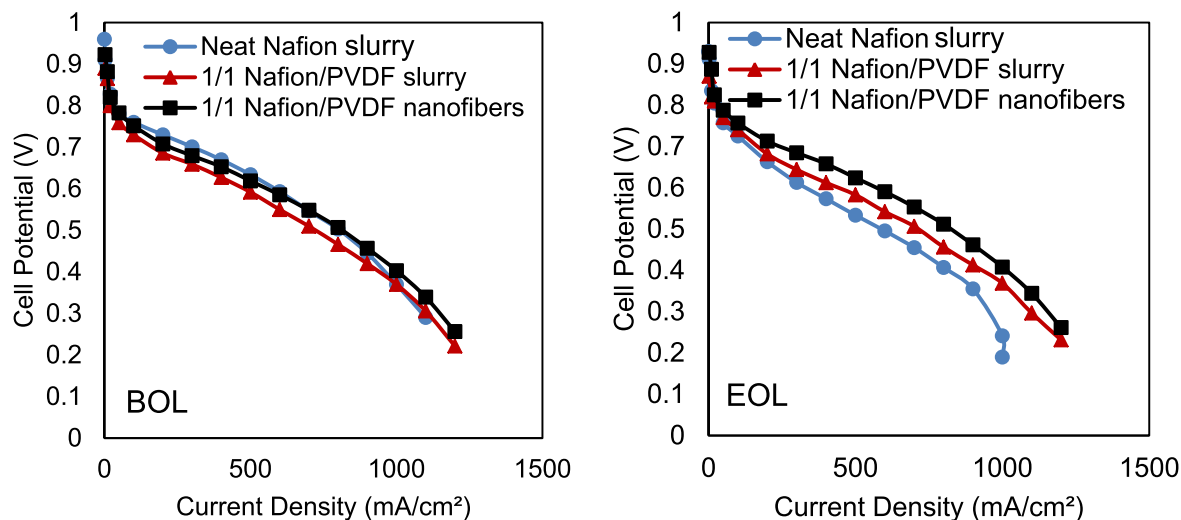


**Figure 5.** Polarization data for neat Nafion electrode, 1/1 Nafion/PVDF slurry electrode, and 1/1 Nafion/PVDF nanofiber electrode MEAs at BOL and EOL (after 1000 carbon corrosion voltage cycles from 1.0 V–1.5 V at 500 mV/s in a triangular wave). All MEAs have a loading of 0.1 mg/cm<sup>2</sup> Pt at the anode and cathode, a Nafion 211 membrane, and a Sigracet 25BC gas diffusion layer. The operating conditions are 80 °C, ambient pressure, and 125/500 sccm H<sub>2</sub>/air feed gas flow rates.

**Table II.** Key cathode performance metrics before and after the carbon corrosion accelerated stress test. Polarization data at ambient pressure, 80 °C, 125/500 sccm H<sub>2</sub>/air. AST conditions: 100% RH, 80 °C, 500 mV/s triangular wave from 1.0 V to 1.5 V 1000 cycles in 100/100 sccm H<sub>2</sub>/N<sub>2</sub>.

	Power Density at 0.65 V (mW/cm <sup>2</sup> )		Cathode thickness (EOL/BOL) %	Cathode Porosity (%)	
	BOL	EOL		BOL	EOL
Neat Nafion Slurry	285	147	49% ± 6.0%	44%	20%
Nafion/PAA nanofibers	402	229	42% ± 8.6%	50%	28%
1/1 Nafion/PVDF Slurry	210	197	99% ± 6.0%	46%	48%
1/1 Nafion/PVDF Fibers	260	261	102% ± 4.3%	45%	52%

**Table III.** Summary electrochemical performance of different cathodes at BOL and EOL (data from Ref. 13).

Pt/C Cathode Type and Binder (w/w)	Cathode ECSA (m <sup>2</sup> /g <sub>Pt</sub> )		Cathode Mass Activity <sup>a)</sup> (A/mg <sub>Pt</sub> )	
	BOL	EOL	BOL	EOL
Neat Nafion slurry	36	21	0.11	0.080
Nafion/PAA nanofibers	45	28	0.16	0.14
1/1 Nafion/PVDF slurry	36	24	0.067	0.077
1/1 Nafion/PVDF nanofibers	44	30	0.093	0.11

a) measurements taken at 0.90 V in O<sub>2</sub> at 7 psi<sub>g</sub> and 100% RH.

it can be concluded that: (1) the difference in EOL power for the Nafion slurry vs Nafion/PVDF slurry MEAs is due to differences in cathode thickness and porosity after voltage cycling (the EOL ECSA and mass activity are nearly the same for these two MEAs), (2) the lower EOL power for the nanofiber cathode MEA with Nafion/PAA binder vs the nanofiber cathode with Nafion/PVDF binder is due to the decrease in cathode thickness and loss of porosity for the former, i.e., the structural changes to the cathode at EOL dominate over mass activity, which is higher for the Nafion/PAA fiber cathode, and (3) the higher EOL power for the nanofiber vs slurry cathode MEA with Nafion/PVDF binder is due to a significantly higher ECSA and oxygen reduction reaction mass activity for the nanofiber cathode MEA. The presence of PVDF in the cathode slows carbon corrosion (due to its hydrophobic property) and it stabilizes the electrode structure and prevents cathode collapse, even as the cathode is losing some carbon and becoming more porous. The retention of electrode thickness/porosity is due to the fact that PVDF has better mechanical

properties than Nafion, i.e., a tensile modulus of ~1.0 GPa at 80 °C vs ~0.05 GPa for hot/wet Nafion 112 at the same temperature.<sup>38,39</sup>

## Conclusions

The impact of polyvinylidene fluoride (PVDF) as a binder component with Nafion perfluorosulfonic acid on the durability of Pt/C cathodes in a proton exchange membrane H<sub>2</sub>/air fuel cell membrane-electrode-assembly (MEA) during a carbon corrosion voltage cycling accelerated stress test (AST) was examined using electrochemical fuel cell performance data and visual inspection/analysis of the cathode morphology via electron microscopy. Electrospun nanofiber cathode mat MEAs with a Nafion/PVDF or Nafion/PAA binder and a slurry cathode MEA with neat Nafion or a Nafion/PVDF binder were investigated. The mechanism of improving fuel cell lifetime (improving durability) with PVDF is two-fold: (1) The presence of PVDF in the cathode binder increases



the hydrophobicity of the electrode, which facilitates the expulsion of water, thus lowering the rate of carbon corrosion, and (2) the presence of PVDF stabilizes the electrode structure and prevents cathode collapse, even as the cathode is losing some carbon and becoming more porous. The presence of PVDF, however, dilutes Nafion ionomer and lowers the proton conductivity of the binder. In the present study, both fiber mat and slurry electrode morphologies with a Nafion/PVDF binder exhibited the following desirable characteristics: (1) the same cathode carbon loss in a carbon corrosion accelerated stress test (AST), that decreased with increasing PVDF content, (2) the retention of beginning-of-life cathode thickness and porosity for Nafion/PVDF binders containing at least 50 wt% PVDF, and (3) minimal/no power loss after the carbon corrosion AST for a 50/50 Nafion/PVDF weight ratio binder. The deleterious effect of PVDF in a Nafion/PVDF cathode binder (i.e., the increase in ionic/proton resistance due to the presence of uncharged PVDF polymer) which severely reduces the power output of a slurry cathode MEA is counterbalanced by the inherent advantages/properties of the nanofiber mat electrode design, i.e., a high electrochemical surface area and a high mass activity at beginning-of-life that persists throughout the carbon corrosion AST.

### Acknowledgments

Work carried out at Oak Ridge National Laboratory and Vanderbilt University, was supported by the U.S. Department of Energy Fuel Cell Technologies Office, through the Fuel Cell Performance and Durability (FC-PAD) Consortium, Dimitrios Papageorgopoulos, Fuel Cells Program Manager, (DOE contract No. DE-EE000765 at Vanderbilt). Vanderbilt researchers were also supported by grants from Merck KGaA and the National Science Foundation, TN-SCORE program (NSF EPS-1004083) under Thrust 2.

### ORCID

Karren L. More  <https://orcid.org/0000-0001-5223-9097>  
Peter N. Pintauro  <https://orcid.org/0000-0001-5115-7276>

### References

1. T. Yoda, H. Uchida, and M. Watanabe, *Electrochim. Acta*, **52**, 5997 (2007).
2. J. Xie, D. L. Wood, D. M. Wayne, T. A. Zawodzinski, P. Atanassov, and R. L. Borup, *J. Electrochem. Soc.*, **152**, A104 (2005).
3. A. S. Aricò, A. Stassi, E. Modica, R. Ornelas, I. Gatto, E. Passalacqua, and V. Antonucci, *J. Power Sources*, **178**, 525 (2008).
4. P. Yu, M. Pemberton, and P. Plasse, *J. Power Sources*, **144**, 11 (2005).
5. K. Matsuoka, S. Sakamoto, K. Nakato, A. Hamada, and Y. Itoh, *J. Power Sources*, **179**, 560 (2008).
6. K. H. Kangasniemi, D. A. Condit, and T. D. Jarvi, *J. Electrochem. Soc.*, **151**, E125 (2004).
7. H. Yoshida, T. Kinumoto, Y. Iriyama, Y. Uchimoto, and Z. Ogumi, *ECS Trans.*, **11**, 1321 (2007).
8. S. Zhang, X. Z. Yuan, J. N. C. Hin, H. Wang, J. Wu, K. A. Friedrich, and M. Schulze, *J. Power Sources*, **194**, 588 (2009).
9. K. Takahashi, R. Koda, K. Kakinuma, and M. Uchida, *J. Electrochem. Soc.*, **164**, F235 (2017).
10. M. K. Debe, A. K. Schmoeckel, G. D. Vernstrom, and R. Atanasoski, *J. Power Sources*, **161**, 1002 (2006).
11. J. Wu, X. Z. Yuan, J. J. Martin, H. Wang, J. Zhang, J. Shen, S. Wu, and W. Merida, *J. Power Sources*, **184**, 104 (2008).
12. L. Dubau et al., *WIREs Energy Environ.*, **3**, 540 (2014).
13. M. Brodt, R. Wycisk, N. Dale, and P. Pintauro, *J. Electrochem. Soc.*, **163**, F401 (2016).
14. W. Zhang and P. N. Pintauro, *ChemSusChem*, **4**, 1753 (2011).
15. M. Brodt, T. Han, N. Dale, E. Niangar, R. Wycisk, and P. Pintauro, *J. Electrochem. Soc.*, **162**, F84 (2015).
16. M. Brodt, R. Wycisk, and P. N. Pintauro, *J. Electrochem. Soc.*, **160**, F744 (2013).
17. R. J. Fairweather, B. Li, R. Mukundan, J. Fenton, and R. L. Borup, *ECS Trans.*, **33**, 433 (2010).
18. N. Macauley, D. D. Papadias, J. Fairweather, D. Spornjak, D. Langlois, R. Ahluwalia, K. L. More, R. Mukundan, and R. L. Borup, *J. Electrochem. Soc.*, **165**, F3148 (2018).
19. B. T. Sneed, D. A. Cullen, K. S. Reeves, O. E. Dyck, D. A. Langlois, R. Mukundan, R. L. Borup, and K. L. More, *ACS Appl. Mater. Interfaces*, **9**, 29839 (2017).
20. J. Wang, G. Yin, Y. Shao, S. Zhang, Z. Wang, and Y. Gao, *J. Power Sources*, **171**, 331 (2007).
21. M. Uchida, Y. Aoyama, N. Eda, and A. Ohta, *J. Electrochem. Soc.*, **142**, 4143 (1995).
22. U.S. DOE Fuel Cell Technologies Office, Section 3.4 Fuel Cells Multi-year research, development, and demonstration Plan, p. 3.4.1, 2016 [https://www.energy.gov/sites/prod/files/2017/05/f34/cto\\_myrd\\_fuel\\_cells.pdf](https://www.energy.gov/sites/prod/files/2017/05/f34/cto_myrd_fuel_cells.pdf).
23. M. Brodt, T. Han, N. Dale, E. Niangar, R. Wycisk, and P. Pintauro, *J. Electrochem. Soc.*, **162**, F84 (2014).
24. H. A. Gasteiger, S. S. Kocha, B. Sompalli, and F. T. Wagner, *Appl. Catal. B Environ.*, **56**, 9 (2005).
25. J. Z. Huamin Zhang, J. Zhang, and J. Wu, *PEM Fuel Cell Testing and Diagnosis* (Elsevier Science, New York) (2013).
26. A. Ohma, K. Shinohara, A. Iiyama, T. Yoshida, and A. Daimaru, *ECS Trans.*, **41**, 775 (2011).
27. P. Soille and L. M. Vincent, *IEEE Trans. on Pattern Analysis and Machine Intelligence*, **13**, 583 (1991).
28. L. Dubau et al., *Int. J. Hydrogen Energy*, **39**, 21902 (2014).
29. K. G. Gallagher, R. M. Darling, and T. F. Fuller, *Handbook of Fuel Cells Volume 6, Part 5: Performance Degradation* (John Wiley & Sons, Ltd, Hoboken, NJ) (2009).
30. T. Abe, H. Shima, K. Watanabe, and Y. Ito, *J. Electrochem. Soc.*, **151**, A101 (2004).
31. Y. C. Park, K. Kakinuma, M. Uchida, D. A. Tryk, T. Kamino, H. Uchida, and M. Watanabe, *Electrochim. Acta*, **91**, 195 (2013).
32. L. Castanheira, W. O. Silva, F. B. Lima, A. Crisci, L. Dubau, and F. Maillard, *ACS Catal.*, **5**, 2184 (2015).
33. A. Kumar and V. Ramani, *ACS Catal.*, **4**, 1516 (2014).
34. A. Kongkanand, Z. Liu, I. Dutta, and F. T. Wagner, *J. Electrochem. Soc.*, **158**, B1286 (2011).
35. J. C. Meier, C. Galeano, I. Katsounaros, J. Witte, H. J. Bongard, A. A. Topalov, C. Baldizzone, S. Mezzavilla, F. Schth, and K. J. J. Mayrhofer, *Beilstein J. Nanotechnol.*, **5**, 44 (2014).
36. H. Schulenburg, B. Schwanitz, N. Linse, G. G. Scherer, A. Wokaun, J. Krbanjevic, R. Grothausmann, and I. Manke, *J. Phys. Chem. C*, **115**, 14236 (2011).
37. J. W. Park, R. Wycisk, and P. N. Pintauro, *J. Membrane Sci.*, **490**, 103 (2015).
38. Arkema Technical Polymers website, <https://extremematerials-arkema.com/en/product-families/kyнар-pvdf-family/physical-and-mechanical-properties/>.
39. Y. Tang, A. M. Karlsson, M. H. Santare, M. Gilbert, S. Cleghorn, and W. B. Johnson, *Mater. Sci. Eng. A*, **425**, 297 (2006).